forum acusticum 2026
8-12 September · Graz, Austria

NONLINEAR-PHASE REGULARISATION FOR REDUCING NONCAUSAL COMPONENTS IN RADIAL FILTERS FOR SPHERICAL MICROPHONE ARRAYS

Nara Hahn and Filippo Maria Fazi

Institute of Sound and Vibration Research, University of Southampton, United Kingdom

Abstract

A radial filter design approach for rigid spherical microphone arrays is proposed, in which nonlinear-phase regularisation is applied selectively. Anticausal poles close to the imaginary axis are reflected into the left half-plane using all-pass filters, reducing slowly decaying noncausal components while preserving the magnitude response. This framework enables flexible control of the trade-off between phase distortion and modelling delay. The resulting temporal structure and group delay are investigated, demonstrating the potential of the proposed approach as an alternative to conventional zero-phase-regularised radial filters.

Keywords: *rigid spherical microphone array, radial filter, Tikhonov regularisation, nonlinear-phase regularisation*

1. Introduction

Spatial sound capture using rigid spherical microphone arrays typically involves radial filtering in the spherical harmonic domain (i) to compensate for scattering effects caused by the rigid sphere and (ii) to map the sound field on the sphere to the plane wave density function [1]–[3]. Due to the ill-conditioned nature of this inverse filtering problem, regularisation is indispensable for stabilising the filters, particularly at low frequencies and high spherical harmonic orders [4]–[9]. Zero-phase regularisation is commonly used to avoid phase distortions, but this results in noncausal pre-ringing of the filters. A modelling delay is therefore required for online processing [8], [10]. Nonlinear-phase regularisation with strictly causal filter design has also been investigated, where phase alignment is achieved using all-pass filters [5], [7]. However, the resulting overall phase distortion remains a challenge.

Corresponding author: *nara.hahn@soton.ac.uk.*

In this contribution, we propose a nonlinear-phase regularisation which is applied selectively to the poles of the zero-phase-regularised radial filters. Compared with the conventional nonlinear-phase design, where every anticausal pole is replaced, this selective approach reduces phase distortion while still substantially lowering the noncausal energy. The number of poles regularised in this way can be chosen to trade off phase distortion against modelling delay, as required by the application.

2. Radial Filter Design

Let us assume that a sound field of interest is modelled as a superposition of plane waves. The sound field captured on the sphere with radius $r = R$ can be expanded in terms of spherical harmonics up to a finite order [11],

$$P(R,\theta,\phi,\omega) = \sum_{n=0}^{N}\sum_{m=-n}^{n} \breve{P}_{nm}(\omega) Y_{nm}(\theta,\phi), \qquad (1)$$

where $Y_{nm}(\theta,\phi)$ denotes the spherical harmonics of order n and degree m evaluated at colatitude $\theta \in [0,\pi]$ and azimuth $\phi \in [0, 2\pi)$, and $\breve{P}_{nm}(\omega)$ the corresponding coefficients. Similarly, the plane wave density function is expanded as

$$B(\vartheta,\varphi,\omega) = \sum_{n=0}^{N}\sum_{m=-n}^{n} \breve{B}_{nm}(\omega) Y_{nm}(\vartheta,\varphi), \qquad (2)$$

with ϑ and φ respectively denoting the colatitude and azimuth of the directions of arrival. The coefficients $\breve{B}_{nm}(\omega)$ are called the Ambisonic signals.

The relationship between the coefficients of the captured sound field and the Ambisonic signals can be written as [3, Ch. 6]

$$\breve{P}_{nm}(\omega) = \frac{4\pi i^{n-1}}{(\frac{\omega}{c}R)^2 h_n'(\frac{\omega}{c}R)} \breve{B}_{nm}(\omega), \qquad (3)$$

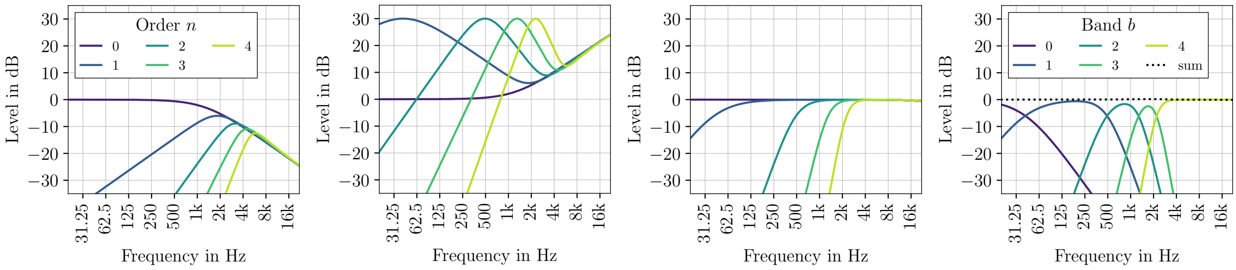

(a) Rigid sphere $H_n(s)$ **(b)** Radial filters $H_n^{\dagger}(s)$ **(c)** Reg. filters $D_n(s)$ **(d)** Filter bank $F_b(s)$

Figure 1: Magnitude responses of (a) the transfer functions on the rigid sphere ($R = 0.042\,\mathrm{m}$), (b) the Tikhonov-regularised radial filters for $G_{\max} = 30\,\mathrm{dB}$, (c) the corresponding regularisation high-pass filters, and (d) the filter bank for spectral compensation. The black dotted line in (d) indicates the sum of the low/band/high-pass filters, where the maximum deviation is 0.2 dB.

where $h_n'(\cdot)$ denotes the derivative of the spherical Hankel function of the second kind. The modal transfer function is given by

$$\frac{\breve{P}_{nm}(\omega)}{\breve{B}_{nm}(\omega)} = \frac{4\pi i^{n-1}}{(\frac{\omega}{c}R)^2 h_n'(\frac{\omega}{c}R)}. \tag{4}$$

In the Laplace domain, the right-hand side can be formulated as [12], [13]

$$4\pi\, e^{\frac{R}{c}s} \frac{\frac{c}{R}s^n}{\prod_{l=1}^{n+1}(s - p_{n,l})}, \tag{5}$$

which exhibits n repeated zeros at $s = 0$ and $n+1$ poles $p_{n,l} \in \mathbb{C}$. Since the scaling factor and the delay are frequency-independent, only the rational part,

$$H_n(s) = \frac{\frac{c}{R}s^n}{\prod_{l=1}^{n+1}(s - p_{n,l})}, \tag{6}$$

will be considered in the following derivation. The factor $\frac{c}{R}$ is kept here so that the 0th-order response $H_0(s)$ has unit magnitude at DC ($s = 0$). The magnitude responses of the modal transfer functions are depicted in Fig. 1(a).

The goal of radial filter design is to find a stable inverse filter of $H_n(s)$. From (5), it is evident that a direct inverse of $H_n(s)$ leads to an unstable filter for orders $n \geq 1$ as it requires repeated poles at $s = 0$. It is a common practice to introduce a regularisation to avoid any excessive amplification of spectral components with low signal energy. Different regularisation approaches have been introduced for the radial filter design to limit the magnitude boost below a prescribed threshold [4], [6], [8], [14].

In this paper, we consider the Tikhonov regularisation, where the regularised inverse is [15]

$$H_n^{\dagger}(s) = \frac{H_n^*(s)}{|H_n(s)|^2 + \lambda} = \frac{1}{H_n(s)} D_n(s), \tag{7}$$

with $(\cdot)^*$ denoting the complex conjugate and $\lambda \in \mathbb{R}^+$ the regularisation parameter. The maximum boost of the regularised inverse can be explicitly controlled by λ via the relation $g_{\max} = 1/(2\sqrt{\lambda})$. The second equality in (7) shows that $H_n^{\dagger}(s)$ can be written as a product of the direct inverse $1/H_n(s)$ (without regularisation) and a regularisation filter $D_n(s)$. Fig. 1(b) and Fig. 1(c) show the magnitude responses of the radial filters and the corresponding regularisation filters for a prescribed maximum gain of $G_{\max} = 20\log_{10}(|g_{\max}|) = 30\,\mathrm{dB}$. It can be seen that the regularisation filters $D_n(s)$ exhibit high-pass filtered characteristics with order-dependent cut-on frequencies and slopes. The poles of the Tikhonov regularisation filters $D_n(s)$, which we denote here by

$$q_{n,l}, \quad l = 1, \ldots, 2n+2, \tag{8}$$

together with their zeros are shown in Fig. 2(a). For each order n, a symmetric pair of real poles with large absolute real parts fall outside the zoomed-in axis limits near $s = 0$ and are therefore not shown. Their distribution is symmetric with respect to the imaginary axis in the Laplace domain, which aligns with the fact that $D_n(s)$ exhibits a zero-phase response [16]. The poles on the left half-plane and right half-plane correspond to the causal and anticausal components of the impulse responses [10].

Due to the order-dependency of the regularisation filters, low-frequency components are gradually attenuated as the order increases. Advanced radial filter design approaches commonly compensate for this spectral imbalance by using a filter bank where each band is encoded with different Ambisonic orders [5], [7], [8], [17]. The filter bank can be constructed by combining the above-mentioned regularisation high-pass filters $D_n(s)$ and their complementary low-pass filters $\bar{D}_n(s) = 1 - D_n(s)$,

$$F_b(s) = \begin{cases} \bar{D}_1(s), & b = 0 \\ D_b(s)\,\bar{D}_{b+1}(s), & b = 1, \ldots, N-1 \\ D_b(s), & b = N. \end{cases} \tag{9}$$

The frequency responses of an exemplary filter bank are shown in Fig. 1(d). Ideally, the sum of the filters

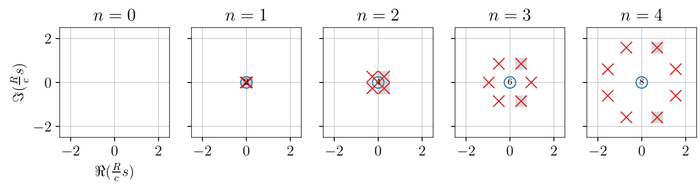

(a) Pole-zero map of $D_n(s)$ ($G_{\max} = 30\,\mathrm{dB}$)

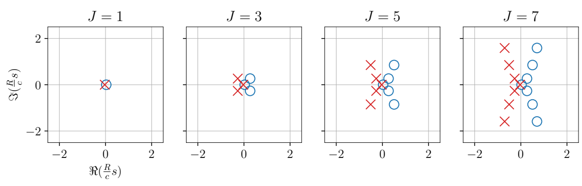

(b) Pole-zero map of $A(s)$ ($G_{\max} = 30\,\mathrm{dB}$)

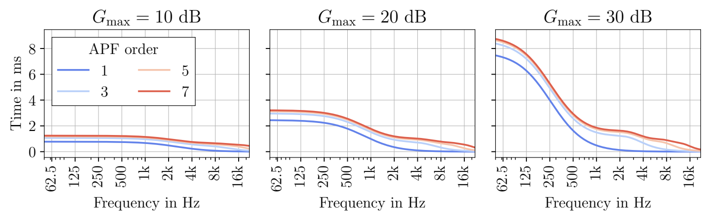

(c) Group delay of the APFs

Figure 2: Design of the APF for nonlinear-phase regularisation. (a) The anticausal poles $q_{n,l}$ are selected from the regularisation filters $D_n(s)$. The filled squares indicate the selected poles for the APF design (cf. Sec. 4). (b) The APF is built by cascading reflected poles and their cancelling zeros $(s - \check{q}_j)/(s + \check{q}_j)$. (c) Group delay of APFs for varying maximum gains $G_{\max} = 10, 20, 30\,\mathrm{dB}$ and APF orders $J = 1, 3, 5, 7$.

$F_b(s)$ (indicated by black dotted line in Fig. 1(d)) must closely match the regularisation filter,

$$D_n(s) \approx \sum_{b=n}^{N} F_b(s). \tag{10}$$

An additional normalisation may be required if the interference between the filters is not negligible [8, Sec. 4]. Finally, the filter bank responses $F_b(s)$ are linearly combined and applied to the direct inverse, yielding the spectrum-compensated radial filters [8],

$$H_n^{\ddagger}(s) = \frac{1}{H_n(s)} \sum_{b=n}^{N} w_{n,b}\, F_b(s), \tag{11}$$

where the weights $w_{n,b}$ depend on the choice of modal weighting (e.g., max-$\boldsymbol{r}_E$ or basic) and equalisation scheme (e.g., omnidirectional, free-field, diffuse-field). More detailed treatment and refinement of the radial filters can be found in [17].

3. Nonlinear-Phase Regularisation

We propose to modify the target frequency response $D_n(s)$, or equivalently the filter bank $F_b(s)$, in such a way that the noncausal components of the output are reduced while keeping the magnitude response unchanged. This constitutes a nonlinear-phase regularisation [18]. Given that the noncausal components are governed by the right-half-plane poles of $D_n(s)$, an effective way to reduce them is to reflect those poles into the left half-plane using an all-pass filter (APF),

$$A(s) = \prod_{j=1}^{J} \frac{s - \check{q}_j}{s + \check{q}_j}, \tag{12}$$

yielding phase-modified regularisation filters,

$$\tilde{D}_n(s) = D_n(s) A(s). \tag{13}$$

The phase-modified filter bank is obtained by applying the APF directly to $F_b(s)$, i.e., $\tilde{F}_b(s) = F_b(s)A(s)$. The real poles or complex conjugate pole pairs $\check{q}_j$ are selected from the anticausal poles of $D_n(s)$,

$$\check{q}_j \in \{q_{n,l} : \Re(q_{n,l}) > 0; n = 0, \ldots, N; l = 1, \ldots, 2n+2\}. \tag{14}$$

The same APF must be applied across all orders to avoid undesired interference when the Ambisonics signals are linearly combined in the decoding stage. The pole-zero cancellation between $A(s)$ and $D_n(s)$ has to be performed explicitly to avoid numerical artefacts in floating-point arithmetic.

A similar approach was introduced in [5], [7] where all anticausal poles were replaced by causal poles, leading to radial filters with strictly causal impulse responses. Our proposed regularisation design, on the other hand, selectively moves the poles according to their decay rate. This enables a flexible design where the overall phase distortion can be controlled based on both the perceptual impact of the phase dispersion and the acceptable modelling delay.

4. Evaluation

To investigate the effect of the nonlinear-phase regularisation, APFs with various orders are implemented. A rigid-sphere microphone array with radius of $R = 0.042\,\mathrm{m}$ is considered. The Ambisonic order is set to $N = 4$. Among 15 anticausal poles of $D_n(s)$ for $n = 0, \ldots, 4$, we choose seven (one real and three complex conjugate pairs) with the smallest real parts. The selected poles are indicated by filled squares in

Fig. 2(a). The APF order was varied from one to seven, by consecutively adding poles with increasing real parts, yielding four nonlinear-phase regularisations ($J = 1, 3, 5, 7$). The corresponding pole-zero distributions are shown in Fig. 2(b). We mainly investigate the properties of the filter bank $F_b(s)$, which is constructed according to (9).

For numerical evaluation, the resulting filter bank is excited by the zero-phase impulse response of an 8th-order Butterworth low-pass filter with a cut-off frequency of 20 kHz. A quasi-continuous time simulation was performed at a sampling frequency of 192 kHz.

The effectiveness of noncausality reduction was quantified in terms of the anticausal energy ratio (AER), defined as

$$\mathrm{AER} = \frac{\int_{-\infty}^{0} |h(t)|^2 \mathrm{d}t}{\int_{-\infty}^{\infty} |h(t)|^2 \mathrm{d}t}, \tag{15}$$

which represents the energy ratio of the noncausal components relative to the overall impulse response. The AER was evaluated by approximating the integrations with summations between $t = -1$ s and $t = +1$ s, for which the impulse responses are sufficiently decayed on both sides of the time axis.

The group delay introduced by the APFs is reported in Fig. 2(c) for maximum amplifications of $G_{\max} = 10\,\mathrm{dB}, 20\,\mathrm{dB}$, and $30\,\mathrm{dB}$. The regularisation with the highest $G_{\max}$ (smallest regularisation parameter λ) results in the largest variation of the group delay across frequencies ranging up to around 9 ms at low frequencies. Stronger regularisations (lower $G_{\max}$) reduce the maximum group delay as well as the overall dispersion. The first APF pole with the smallest real part has the most significant effect on the group delay, whereas the other APF poles contribute to a lesser extent.

Fig. 3 shows the log-amplitude of the filter bank ($F_b(s)$) impulse responses. The impulse responses are derived by using the partial fraction expansion of the Laplace transform and then performing the bilateral inverse Laplace transform [19, Sec. 5.5]. The AER of the impulse response is indicated at the top left corner of each plot. The case of zero-phase regularisation is shown in Fig. 3(a) where the impulse responses exhibit symmetric log-amplitude with respect to $t = 0$ and thus have AERs of 50 % regardless of the ambisonic order. The temporal structure of the impulse responses clearly changes for nonlinear-phase regularisations as shown in Fig. 3(b), 3(c), 3(d), and 3(e). Overall, the noncausal components decay much faster towards the negative time axis, suggesting that the resulting radial filters can be well approximated by truncating the impulse responses with less noncausal length. Moving the first anticausal pole with the smallest real part (cf. Fig. 2(b)) into the left half-plane considerably reduces the noncausal components in band $b = 0$, from 50.0 % to 0.0 %, and to a lesser extent in band $b = 1$ by 3.9 %. Increasing the APF order further reduces the energy of the noncausal components as confirmed by

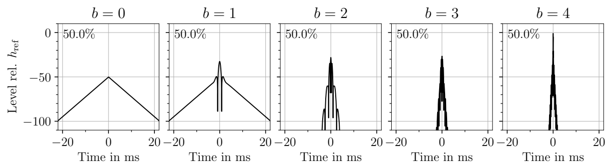

(a) Linear-phase

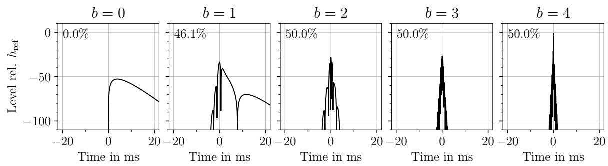

(b) Nonlinear-phase (1st order APF)

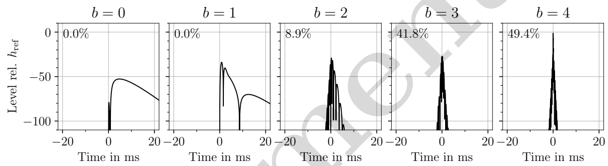

(c) Nonlinear-phase (3rd order APF)

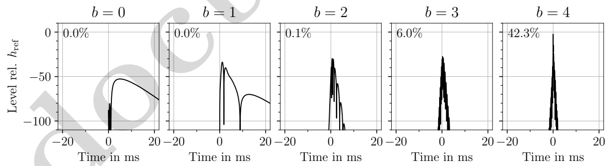

(d) Nonlinear-phase (5th order APF)

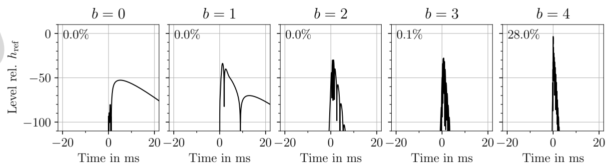

(e) Nonlinear-phase (7th order APF)

Figure 3: Log-amplitude of the filter bank impulse responses ($G_{\max} = 30\,\mathrm{dB}$). The plotted levels are normalised against the peak value of the Butterworth low-pass pulse h_{ref} (8th-order, 20 kHz cut-off). The AER (cf. (15)) is indicated at the top left corner in each panel.

the indicated AERs. For the 7th-order all-pass filter (cf. Fig. 3(e)), the AERs are close to 0.0 % except for band $b = 4$ for which the anticausal components are associated with the remaining poles on the right half-plane, cf. Fig. 2(a).

5. Conclusion

The proposed approach for nonlinear-phase regularisation was shown to reduce the noncausal components of the radial filters effectively. This advantage is expected to allow a radial filter design with smaller modelling delay. The flexible selection of APF order also enables control of the overall phase distortion to some extent. Preliminary evaluations also revealed how the nonlinear-phase regularisation and the maximum boost influence the temporal structure and the group delay exhibited by the radial filters.

In practice, the radial filter with nonlinear-phase regularisation can be implemented either by FIR filters similar to the approach presented in [8] or by combining FIR and IIR filters which involves forward-and-backward filtering [10], [20]. Whether the resulting phase distortion leads to perceivable timbral colouration remains to be investigated by assessing the auralised sound via loudspeakers or headphones. The perceptual impact may be highly dependent on the regularisation parameter, which was shown to have considerable impact on the group delay. Also of interest is how the nonlinear-phase response interacts with the spatial aliasing components which exhibit distinct spectral and temporal structure [21]. Both topics remain for future work.

References

[1] J. Meyer and G. Elko, “A highly scalable spherical microphone array based on an orthonormal decomposition of the soundfield”, in *Proc. Int. Conf. Acoust. Speech Signal Process. (ICASSP)*, Orlando, FL, USA, May 2002.

[2] B. Rafaely, *Fundamentals of Spherical Array Processing*. Berlin, Germany: Springer, 2015.

[3] F. Zotter and M. Frank, *Ambisonics*. Cham, Switzerland: Springer, 2019.

[4] S. Moreau, J. Daniel, and S. Bertet, “3D sound field recording with higher order ambisonics–objective measurements and validation of a 4th order spherical microphone”, in *Proc. 120th Audio Eng. Soc. (AES) Conv.*, Paris, France, May 2006.

[5] R. Baumgartner, H. Pomberger, and M. Frank, “Practical implementation of radial filters for ambisonic recordings”, in *Proc. of Int. Conf. Spatial Audio (ICSA)*, Detmold, Germany, Apr. 2011.

[6] B. Bernschütz, C. Pörschmann, S. Spors, and S. Weinzierl, “Soft-limiting der modalen amplitudenverstärkung bei sphärischen mikrofonarrays im plane wave decomposition verfahren”, in *Proc. 37th German Annu. Conf. Acoust. (DAGA)*, Düsseldorf, Germany, Mar. 2011, pp. 661–662.

[7] S. Lösler and F. Zotter, “Comprehensive radial filter design for practical higher-order ambisonic recording”, in *Proc. 41st German Annu. Conf. Acoust. (DAGA)*, Nuremberg, Germany, Mar. 2015, pp. 452–455.

[8] F. Zotter, “A linear-phase filter-bank approach to process rigid spherical microphone array recordings”, in *Proc. Int. Conf. Electron. Telecommun. Comput. Automat. Nuclear Eng. (ETRAN)*, Palić, Serbia, 2018.

[9] C. Langrenne, E. Bavu, and A. Garcia, “A linear phase IIR filterbank for the radial filters of ambisonic recordings”, in *Proc. EAA Spatial Audio Signal Process. Symp.*, Paris, France, Sep. 2019, pp. 127–132.

[10] N. Hahn and F. M. Fazi, “IIR implementation of tikhonov-regularised radial filters for rigid spherical microphone arrays”, in *Proc. 52nd German Annu. Conf. Acoust. (DAGA)*, Dresden, Germany, Mar. 2026.

[11] E. Williams, *Fourier Acoustics: Sound Radiation and Nearfield Acoustical Holography*. London, UK: Academic Press, 1999.

[12] H. Pomberger, “Angular and radial directivity control for spherical loudspeaker arrays”, Master’s thesis, University of Music and Dramatic Arts, Graz, Austria, 2008.

[13] N. Hahn, F. Schultz, and S. Spors, “Spatio-temporal properties of simulated impulse responses on a rigid sphere”, in *Proc. 47th German Annu. Conf. Acoust. (DAGA)*, Wien, Austria, Aug. 2021, pp. 836–839.

[14] J. Meyer and G. Elko, “A qualitative analysis of frequency dependencies in ambisonics decoding related to spherical microphone array recording”, in *Proc. Int. Audio Eng. Soc. (AES) Conf.*, Guildford, UK, Jul. 2016.

[15] A. N. Tikhonov and V. Y. Arsenin, *Solutions of Ill-Posed Problems*, trans. by F. John. Washington D.C., USA: V. H. Winston & Sons, 1977.

[16] N. Hahn and F. M. Fazi, “Regularized inverse filter design for rigid spherical microphone array processing: Laplace- and time-domain representations”, in *Proc. Int. Conf. Acoust. Speech Signal Process. (ICASSP)*, Barcelona, Spain, May 2026.

[17] F. Zotter, “Filterbank rule for spherical microphone array encoding and EQs for above aliasing, transducers, and binaural playback”, in *Proc. 156th Audio Eng. Soc. (AES) Conv.*, Madrid, Spain, Jun. 2024.

[18] S. G. Norcross, M. Bouchard, and G. A. Soulodre, “Inverse filtering design using a minimal-phase target function from regularization”, in *Proc. 121st Audio Eng. Soc. (AES) Conv.*, San Francisco, CA, USA, Oct. 2006.

[19] B. Girod, R. Rabenstein, and A. Stenger, *Signals and Systems*. New York, NY, USA: Wiley, 2001.

[20] S. R. Powell and P. M. Chau, “Time reversed filtering in real-time”, in *Proc. IEEE Int. Symp. Circuits Systems*, 1990, pp. 1239–1243.

[21] Y. Li, F. M. Fazi, and N. Hahn, “Time-domain behaviour of spatial aliasing artefacts in spherical microphone array processing”, in *Proc. 12th Conv. Eur. Acoust. Assoc.*, Graz, Austria, Sep. 2026.